

Capillary pressure prediction for fluid surrounding a cylindrical pillar representing an idealized rock structure in porous media

Afshin Davarpanah, Simon Cox*

Department of Mathematics, Aberystwyth University, Aberystwyth SY23 3BZ, United Kingdom

**Correspondence to: foams@aber.ac.uk*

Abstract

Fluid flow in porous media is a complex phenomenon that depends on the reservoir characteristics. Due to the pore size distribution in underground formations, accurate prediction of capillary pressure for various pore shapes and sizes is necessary to understand how changes to the capillary pressure arise. Here we consider the situation in which a small volume of liquid phase surrounds a cylindrical pillar and predict the capillary pressure. We validate our prediction by comparing with Surface Evolver simulations for a range of contact angles and pillar radii.

Keywords: Interface shape; Capillary pressure; Porous media; Oil Recovery; Contact angle.

1. Introduction

The wetting of a solid by a liquid phase occurs in various porous media situations, such as during enhanced oil recovery, stimulation of plugged wells, trapping CO₂ in CO₂ sequestration, and environmental remediation [1]. Capillary forces can cause the spontaneous imbibition of the liquid phase into micro or nano-sized pores in porous media. Therefore, it is important to have a good understanding of the liquid structure in a porous medium since this gives direct information about the processes necessary to extract the liquid and the likely yield.

Wetting behavior is described by the contact angle(s) at which interfaces meet, for example, between the solid and the liquid and between the air and the liquid. The most important parameter governing the feasibility of, say, oil recovery is the capillary pressure (P_c). This is the difference in pressure between two phases coexisting in the porous medium and depends upon inter alia, each phase's volume, relative surface tensions (or contact angles), and pore geometry [2-6]. When regions of different fluids meet, the capillary pressures must equilibrate, and this will determine if the fluid will remain trapped in the complex geometry or whether it can be recovered.

We consider a simple pore geometry here and seek to predict the capillary pressure, deriving an approximate solution of the Young-Laplace Law [3] to compare with accurate Surface Evolver simulations. We explore in particular the effect of different contact angles on the shape and extent of the meniscus surrounding a vertical pillar representing an idealized rock structure.

2. Geometry and methods

2.1. Geometry

Our idealized porous medium consists of an upright circular cylinder with radius \hat{R} spanning the gap between two flat horizontal parallel surfaces with separation \hat{H} . The gap between the surfaces is filled with air except for a narrow meniscus of liquid around the top and bottom of the cylinder. We assume that the gap between the surfaces is smaller than the capillary length, so that we can neglect the effects of gravity. Then by symmetry we need only consider the lower half of this geometry, as shown in Figure 1. Since we expect the size of rock pores to be of order microns while the capillary length is of order millimeters, this is likely to be a good

approximation. At such a scale, we expect capillary pressures to be of order $\hat{\gamma}/\hat{H}$, where $\hat{\gamma}$ is the interfacial tension, of order $30 \times 10^{-3} \text{ Nm}^{-1}$.

As the liquid volume varies, the capillary pressure will vary from small values at large volumes, where the radius of curvature in the (r,z) plane is large, to much larger values at small volumes. Where the liquid meets the cylinder and where it meets the plate it does so at a particular angle, the contact angle. The contact angle is affected by the properties of the liquid and the surfaces it contacts, so it could be different on the cylinder and the substrate. For simplicity, we take these two values to be the same, but the results described below are straightforward to generalise to the case where they are different.

The contact angle is directly related to the balance between the surface tension γ of the liquid-air interface and the surface tension γ_w of the wetting film on the solid walls. If we denote the contact angle by θ_c then

$$\cos\theta_c = \frac{\gamma_w}{\gamma}. \quad (1)$$

Figure 2 defines the contact angle at the upper and lower limits of the liquid meniscus.

The shape of the interface is given by a solution of the Young-Laplace Law [3, 7], which balances the capillary pressure with the local mean curvature at each point of the interface. In this cylindrical geometry, the expression for the curvature is highly non-linear: it has two components, consisting of the principal radii of curvature in two perpendicular directions, and these both vary with vertical position within the meniscus. Our prediction of the capillary pressure will therefore be an approximation, which performs best for large rock structures within

the porous medium ($\hat{R} \gg \hat{H}$), and so to determine how accurate our prediction is we will compare it with precise numerical solutions.

2.2. Numerical method

We work in dimensionless coordinates, with all lengths scaled by the gap height \hat{H} . We define the dimensionless cylinder radius to be $R = \hat{R}/\hat{H}$ and choose a dimensionless surface tension $\hat{\gamma} = 1$. Then a dimensionless capillary pressure of $P_c = 1$ in our results below corresponds to a dimensional capillary pressure of $\hat{\gamma}/\hat{H} \approx 30 \times 10^{-3} / 10^{-6} = 10^3$ Pa.

To perform the simulations we use Surface Evolver [8], which finds the shape of fluid surface shapes with given surface tension and other energies under various constraints. Similar calculations have been performed for small pockets of liquid trapped between spheres [9]. The situation that we consider is axisymmetric so that we need only consider the shape of the interface in the (r,z) plane (see Figure 2). Therefore, the interface consists of a curve connecting the cylinder to the substrate with the given contact angle at each end and a specified enclosed volume.

This curve is discretized into roughly 2^5 straight elements with tension γ . The contact angles are considered as further energies, and the system is evolved to a minimum of energy using a gradient descent method. In the simulations, it is straightforward to vary the cylinder radius R , the liquid volume V and the contact angle θ_c to explore all relevant parameters.

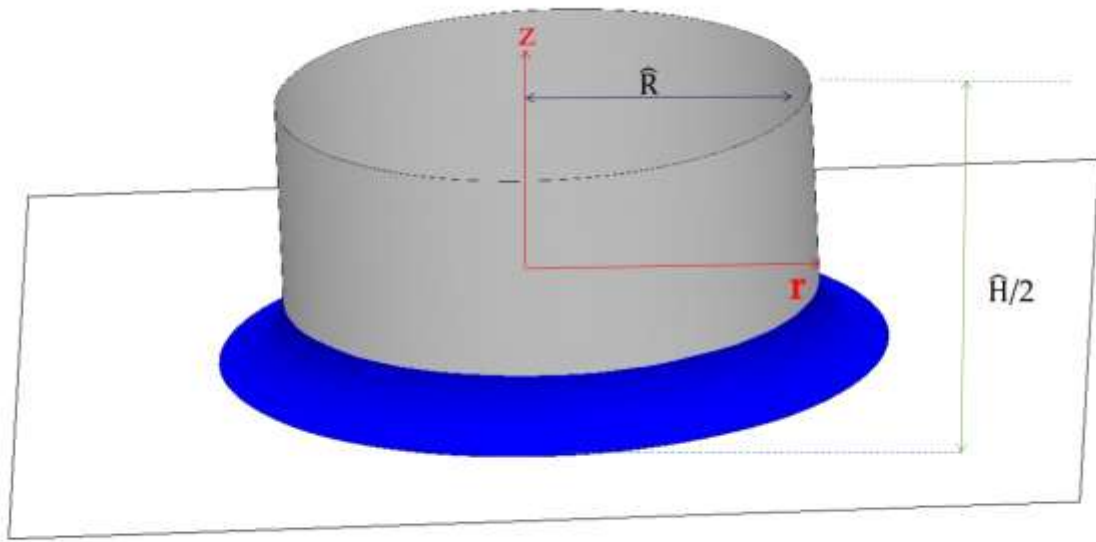


Figure 1. Liquid surrounds the base of a circular cylinder representing an idealized rock structure in a porous medium.

2.3. Capillary pressure prediction

In this simplified geometry, we can derive an approximate formula for the capillary pressure. The Young-Laplace equation for an interface at equilibrium without gravity is

$$P_c = P_{air} - P_{Liquid} = \gamma C \quad . \quad (2)$$

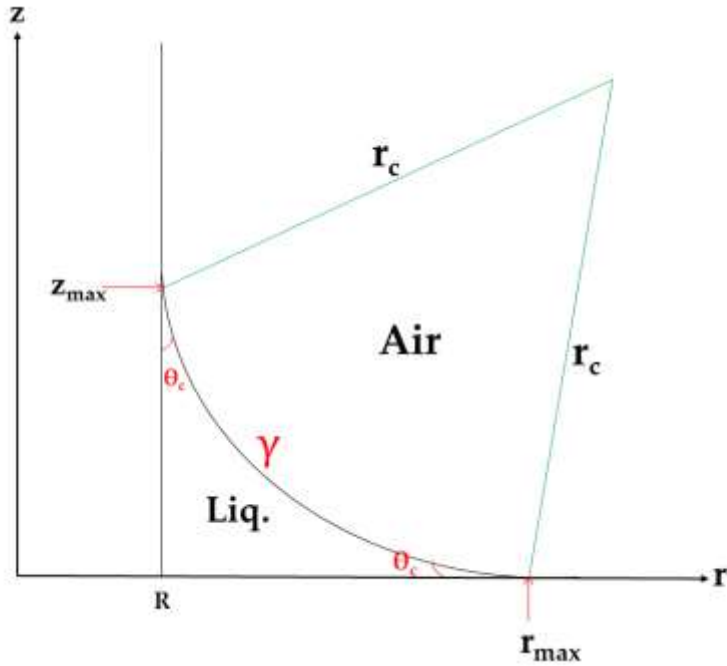


Figure 2. A schematic for a cross-section through the meniscus shape in the (r,z) plane. We consider the case where the contact angles θ_c on the cylinder and the substrate are equal. The interface has radius of curvature r_c , surface tension γ , extent r_{\max} in the radial direction, and height z_{\max} .

The curvature C of the interface can be written [10]:

$$[1 + r_z^2]^{-3/2} \left(-r_{zz} + \frac{1+r_z^2}{r} \right) = -C \quad , \quad (3)$$

which is valid for $\theta < \frac{\pi}{4}$. This expression is too complex to find a closed-form solution. Instead, we assume that in typical porous media, the size of the rock structures is large, $R \gg 1$. Then the second term in parentheses in (3), containing the factor $1/r$, will be dominated by the first, and we choose to neglect it. As we shall see below, we are effectively approximating the interface as a circular arc (precisely one-quarter of a circle if $\theta_c = 0$) in the (r,z) plane.

Above a contact angle of $\frac{\pi}{4}$ the curvature of the interface will change sign. The capillary pressure will also go from positive to negative, i.e., the liquid pressure will exceed the air pressure. To accommodate this change, we write eq. (2) as

$$[1 + r_z^2]^{-\frac{3}{2}} r_{zz} = \text{sign}\left(\frac{\pi}{4} - \theta_c\right) \frac{P_c}{\gamma} \quad (4)$$

We now seek a solution of (4).

2.3.1 Predicting the Interface Shape

Following Teixeira et al. (2015), we introduce the coordinate θ with $\cot\theta = -r_z$ in Eq. (4) to give

$$\sin\theta \frac{d\theta}{dz} = \text{sign}\left(\frac{\pi}{4} - \theta_c\right) \frac{P_c}{\gamma} \quad (5)$$

Integrating gives the height of the interface in terms of the parameter θ :

$$z(\theta) = \frac{P_c}{\gamma} (\cos\theta_c - \cos\theta) \quad \text{with} \quad \theta \in \left(\theta_c, \frac{\pi}{2} - \theta_c\right) \quad , \quad (6)$$

although P_c remains unknown at this stage. The maximum height reached by the meniscus on the cylinder occurs when $\theta = \frac{\pi}{2} - \theta_c$:

$$z_{max} = \frac{P_c}{\gamma} (\cos\theta_c - \sin\theta_c). \quad (7)$$

This expression is shown in Figure 5 below, which we describe once the value of P_c is predicted.

Since the interface is now approximated by an arc of a circle, the maximum extent of the meniscus in the radial direction is

$$r_{max} = R + \frac{P_c}{\gamma} (\cos\theta_c - \sin\theta_c). \quad (8)$$

We now replace θ from Eq. (5) using $\cot\theta = \frac{\cos\theta}{\sqrt{1-\cos^2\theta}} = -\frac{dr}{dz}$ to find the interface profile $z(r)$. We

integrate

$$-\frac{dr}{dz} = \frac{\cos\theta_c - \frac{P_c z}{\gamma}}{\sqrt{1 - \left(\cos\theta_c - \frac{P_c z}{\gamma}\right)^2}}$$

to obtain

$$\left(z - \frac{\gamma \cos\theta_c}{P_c}\right)^2 + \left(r - \left(R + \frac{\gamma \cos\theta_c}{P_c}\right)\right)^2 = \left(\frac{\gamma}{P_c}\right)^2. \quad (9)$$

Clearly, this is the equation of a circle with radius $\frac{\gamma}{P_c}$ and centre $(R+r_c, r_c)$, where $r_c = \gamma \cos\theta_c / P_c$.

The radius of curvature increases, and the meniscus gets larger, as the capillary pressure decreases, as expected. As the contact angle changes the centre of curvature moves closer to the axes, but we have yet to determine the effect on the capillary pressure of changes in the contact angle, which we do next.

2.3.2 Predicting the capillary pressure

Let us assume that R , θ_c and γ are given. We need to find the capillary pressure P_c to completely solve the problem, which we do by determining the liquid volume $V = 2\pi \int_R^{R+r_c(1-\tan\theta_c)} z r dr$

with $z(r)$ from Eq. (9).

The substitution $r = R + r_c \left(1 - \frac{\cos\theta}{\cos\theta_c}\right)$ allows us to resolve the integral:

$$V = 2\pi r_c^2 \left\{ R \left[1 - \tan\theta_c - \left(\frac{\pi - \theta_c}{\cos^2\theta_c}\right) \right] + r_c \left[\frac{(1 - \tan\theta_c)^2}{2} - \left(\frac{\pi - \theta_c}{\cos^2\theta_c}\right) + \frac{1 - \tan^3\theta_c}{3} \right] \right\}. \quad (10)$$

In keeping with our assumption that R is large, we retain only the first term¹, proportional to $r_c^2 R$, and neglect the second term proportional to r_c^3 :

$$V \approx 2\pi r_c^2 R \left[1 - \tan\theta_c - \frac{\frac{\pi}{4} - \theta_c}{\cos^2\theta_c} \right] = 2\pi \left(\frac{P_c}{\gamma} \right)^2 R \left[\cos^2\theta_c - \frac{1}{2}\sin 2\theta_c + \theta_c - \frac{\pi}{4} \right]. \quad (11)$$

Introducing the function $f(\theta_c) = \cos^2\theta_c - \frac{1}{2}\sin 2\theta_c + \theta_c - \frac{\pi}{4}$ for the dependence on the contact angle then gives

$$P_c \approx \text{sign}\left(\frac{\pi}{4} - \theta_c\right) \gamma \sqrt{\frac{2\pi R f(\theta_c)}{V}} \quad (12)$$

We consider volumes V that are small enough that $z_{\max} < H/2$ so that the liquid regions around the top and bottom of the cylinder never meet.

3. Results

3.1 Interface Shape

The volume of the meniscus is approximately its cross-sectional area multiplied by the circumference of the cylinder. Therefore, in the following, we consider liquid volumes that scale with R , with the expectation that the cross-section of the meniscus remains roughly constant in shape.

Figure 3 shows that the interface does indeed become closer to a circle as R increases. The data is shown for a representative small contact angle of $\frac{\pi}{18}$. For $R \leq 1$ there is a clear deviation from

¹ Given the dependence of r_c on ΔP , Eq. (10) is a cubic for ΔP of the form $a\Delta P^3 + b\Delta P^2 - c = 0$, which could be solved to give $P_c(V)$

the predicted circle, but for $R=5$ and $R=50$ the simulation results are almost indistinguishable from our prediction.

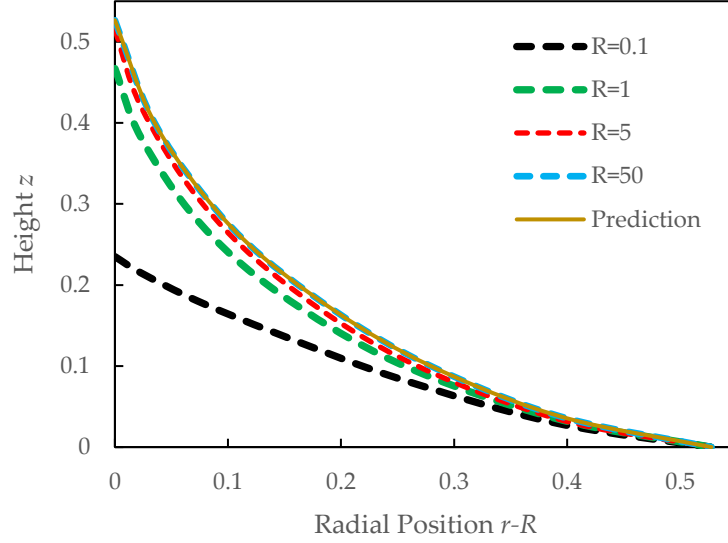


Figure 3. Interface shapes for different pillar radius, with $V = 0.5R$ and $\theta_c = \frac{\pi}{18}$. Simulation data is compared with our prediction, eq. (9), with P_c given by eq. (12).

As R increases, the height of the meniscus increases towards the prediction of Eq. (7) until the circular shape is reached at large R . Our prediction does not capture this variation, but Figure 4 does show that for R greater than about 20, the prediction is very good, within a few percent.

More remarkable is that the extent of the meniscus r_{\max} appears constant as the radius of the cylinder varies. This is shown in Figure 4 for $\theta_c = \frac{\pi}{18}$, indicating close agreement between our prediction (Eq. 8) and the numerical data.

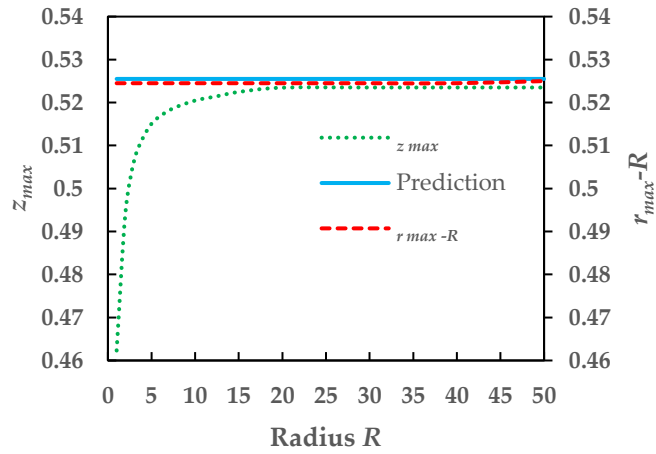


Figure 4. The extent of the meniscus ($r_{max}-R$ and z_{max}) for volume $V=0.5R$ at $\theta_c = \frac{\pi}{18}$.

However, varying the contact angle (Figure 5) indicates that (i) for large R , both z_{max} and r_{max} are accurately predicted; (ii) for $R=1$, the prediction overestimates r_{max} significantly for all contact angles; and (iii) the error in r_{max} changes sign around $\frac{\pi}{18}$, although it is much smaller in magnitude than the error in z_{max} .

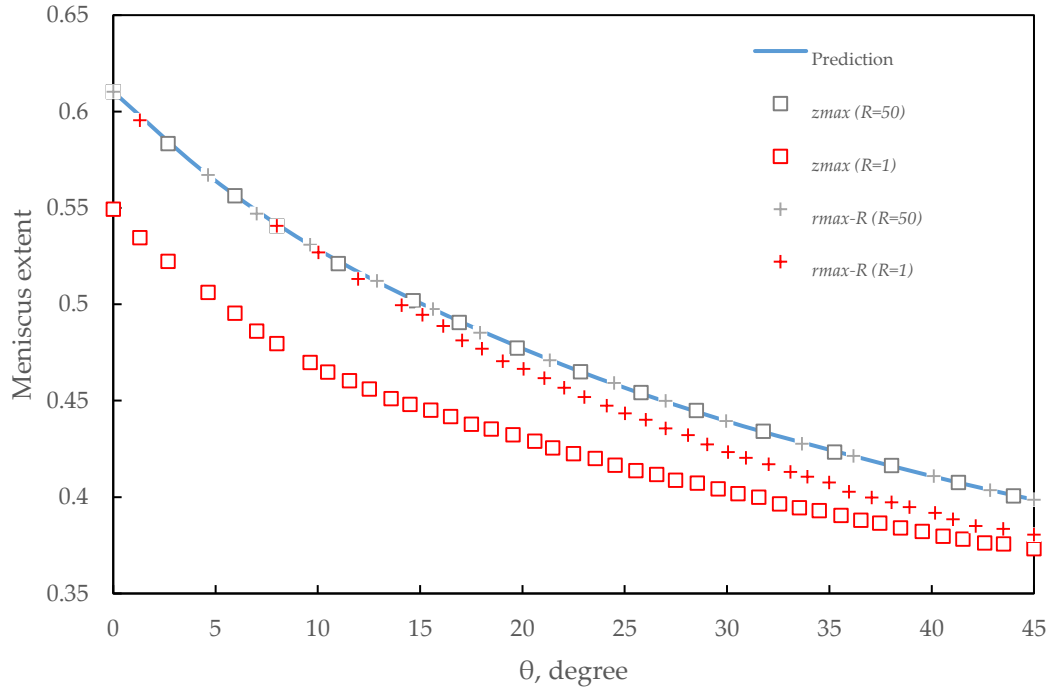


Figure 5. The extent of the meniscus in the horizontal ($r_{\max} - R$, + symbols) and vertical (z_{\max} , diamonds) directions as a function of contact angle for fixed volume ($V=0.5R$). Data for the cases $R=1$ (red symbols) and $R=50$ (grey symbols) are compared with the predictions Eqs. (7) and (8).

3.2. Capillary pressure

3.2.1 Effect of pillar radius

Figure 6 shows that with liquid volume varying linearly in cylinder radius ($V = 0.5R$) and the contact angle fixed at $\frac{\pi}{18}$ the capillary pressure increases with R . In this respect, the capillary pressure follows a similar trend to z_{\max} : as R increases, the capillary pressure converges towards our prediction. Although the prediction for P_c is within 10% for $R \approx 2$, it is not until larger R , close to 20, that the prediction is within about 1%.

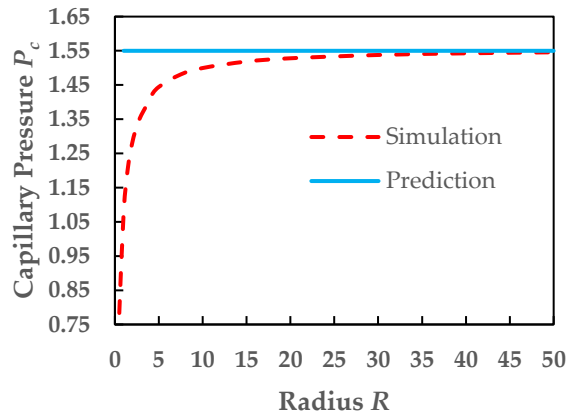


Figure 6. Effect of pillar radius on capillary pressure for linearly increasing volume ($V=0.5R$) with contact angle $\theta_c = \frac{\pi}{18}$.

Again for $\theta_c = \frac{\pi}{18}$, Figure 7 shows the capillary pressure for a range of values of R . In each case, the capillary pressure decreases as the meniscus volume increases, most steeply for small liquid volumes.

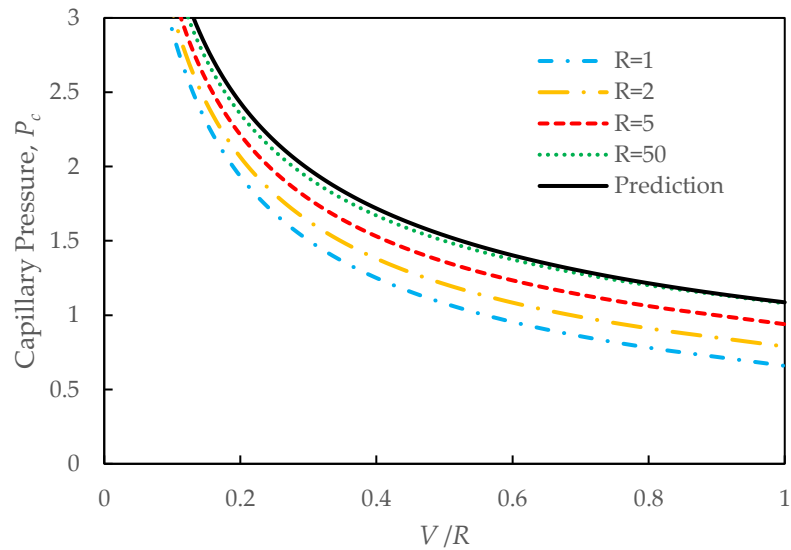


Figure 7. Effect of pillar radius on capillary pressure for a range of volumes with contact angle $\theta_c = \frac{\pi}{18}$.

Note that the horizontal axis for volume is scaled by the cylinder radius R for convenience.

3.2.2 Effect of contact angle

Interface shapes are shown in Figure 9(a) for different contact angles. As the contact angle increases, the curvature reduces.

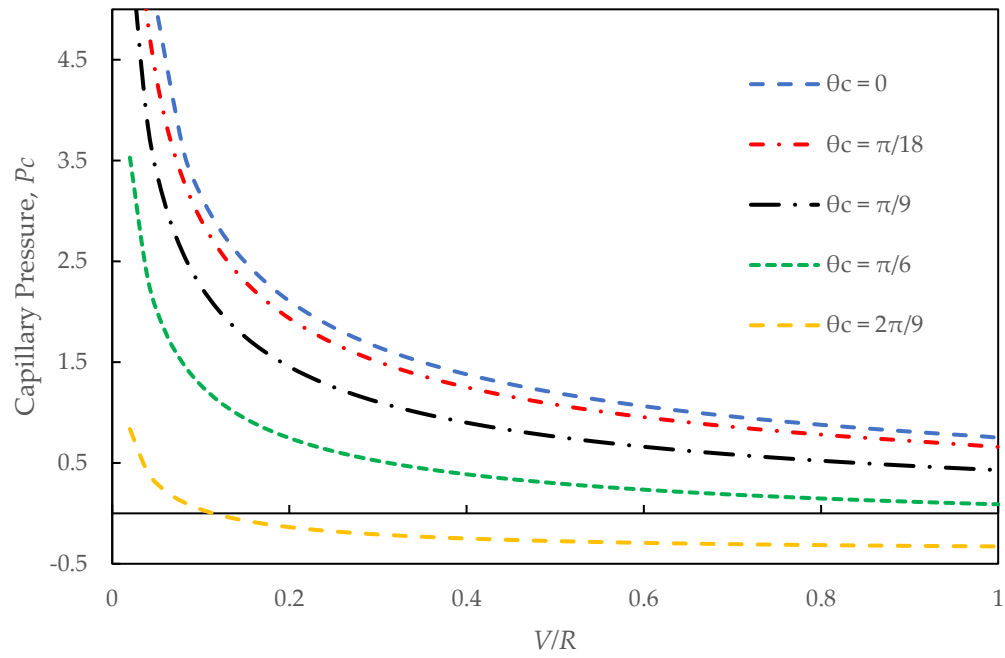
The same trend of decreasing capillary pressure with increasing volume is observed for all contact angles (Figure 8) and all meniscus volumes (Figure 9). We see that the highest pressures are found for the smallest contact angles, since as the contact angle increases, the interface straightens out, and for the smallest liquid volumes, since the interface is more strongly curved closer to the cylinder. The same data is used to determine the error in the prediction, calculated according to

$$\varepsilon(P_c) = P_c(\text{data}) - P_c(\text{pred}) . \quad (13)$$

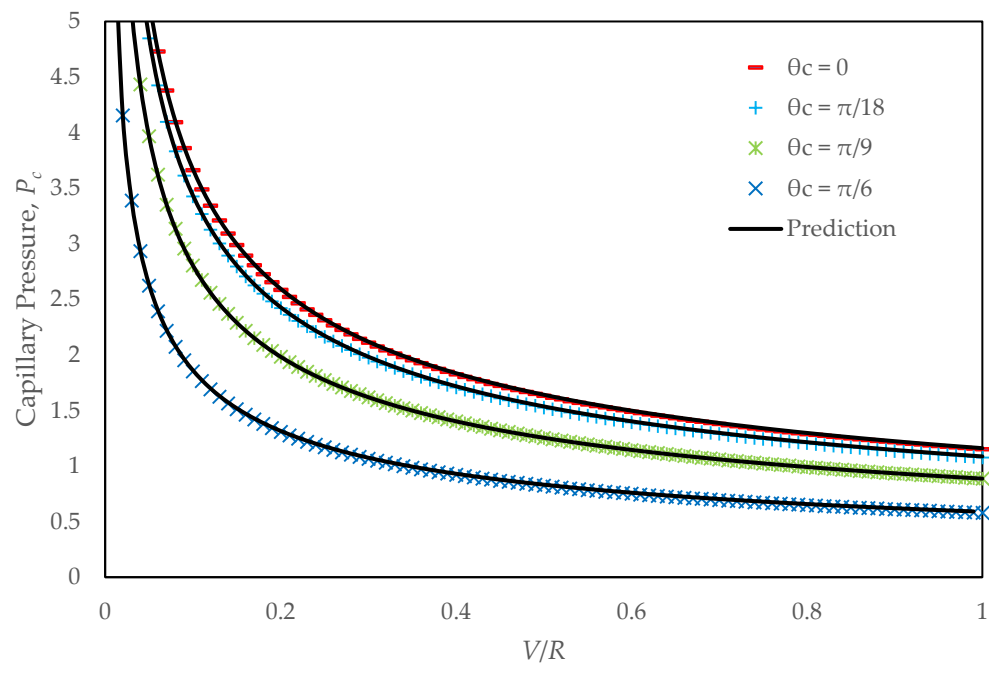
This is shown in Figure 8c: the error increases with the liquid volume at different contact angles and the error decreases with increasing volume.

For certain values of the contact angle and liquid volume, the capillary pressure can change sign; an example is shown in Figure 8(a) for $R=1$ and $\theta_c = \frac{2\pi}{9}$. As R increases, we expect this cross-over value to converge on $\theta_c = \frac{\pi}{4}$ for any meniscus volume (Figure 9(c)), but for smaller R the critical contact angle decreases as the meniscus volume increases (Figure 9(b)). Thus for sufficiently small volumes the critical contact angle at which the capillary pressure changes sign

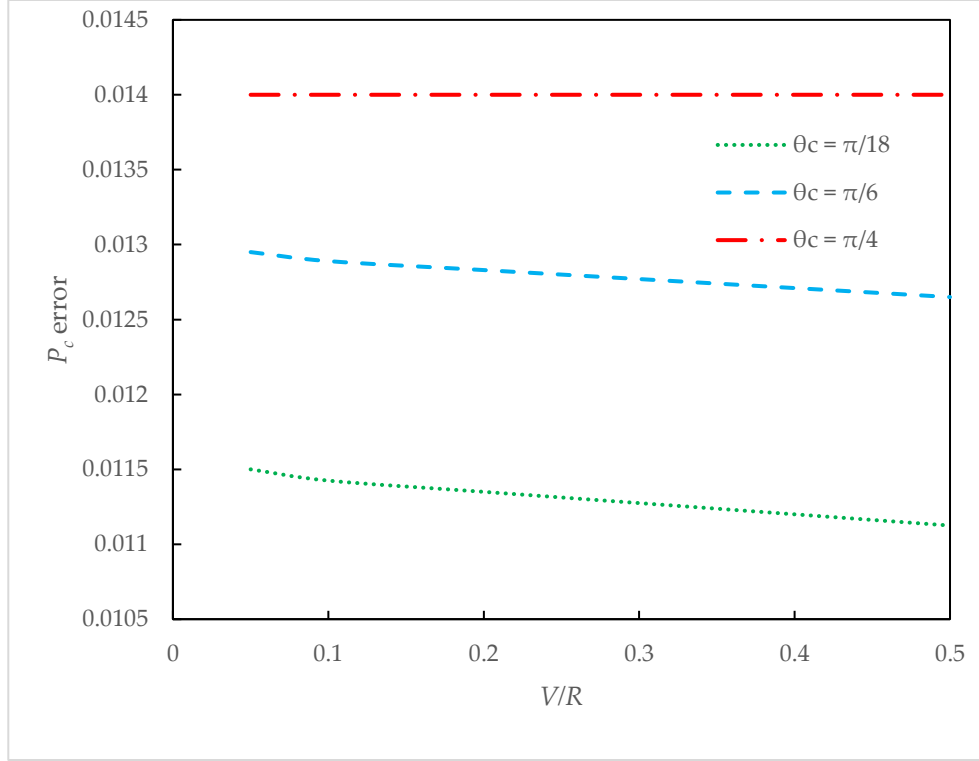
is still $\frac{\pi}{4}$. (At very large volumes it is probably necessary to include gravity in the calculation, so we refrain from hypothesising on the behaviour in this limits.)



(a)



(b)

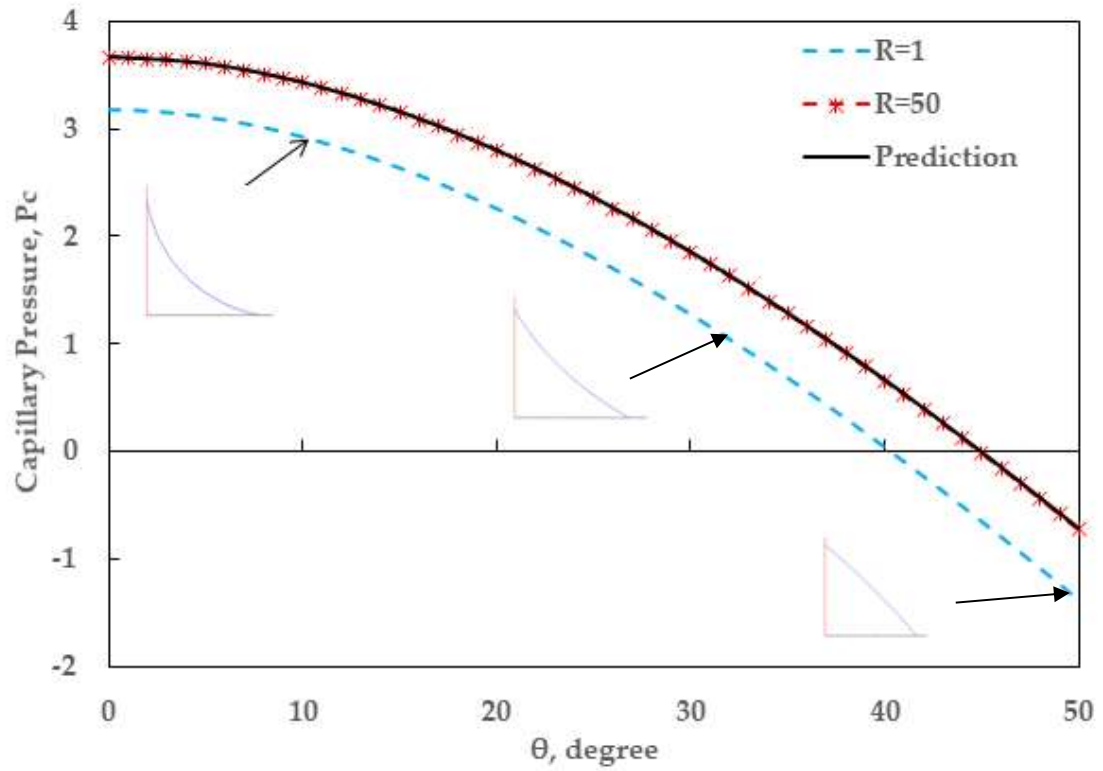


(c)

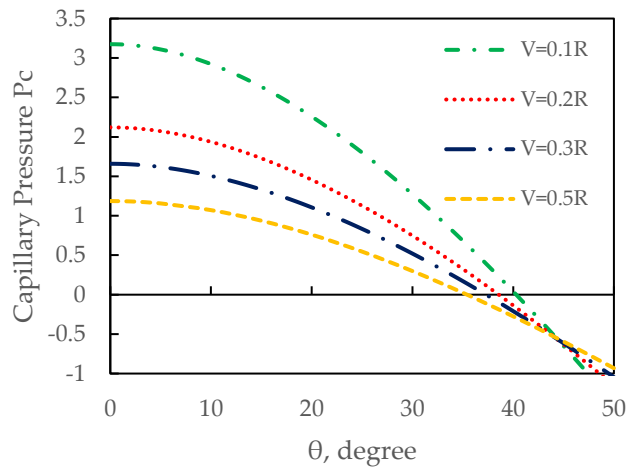
Figure 8. Effect of contact angle on capillary pressure for (a) $R=1$ and (b) $R=50$. (c) The percentage error in the capillary pressure, calculated according to Eq. 13, for the case $R=50$.

Figure 9(a) shows that our prediction of the capillary pressure is indistinguishable from the data for all values of the contact angle for large cylinders ($R=50$) and that it is within about 10% for $R=1$. Figures 9(b) and 9(c) suggest that there is a particular contact angle at which the capillary pressure is independent of the liquid volume for given radius R . This occurs at $\theta_c = \frac{\pi}{4}$ for large R , since the interface is flat (in the (r,z) plane). For smaller R , it occurs at smaller θ_c where the interface curvature has changed sign and it bulges outwards slightly.

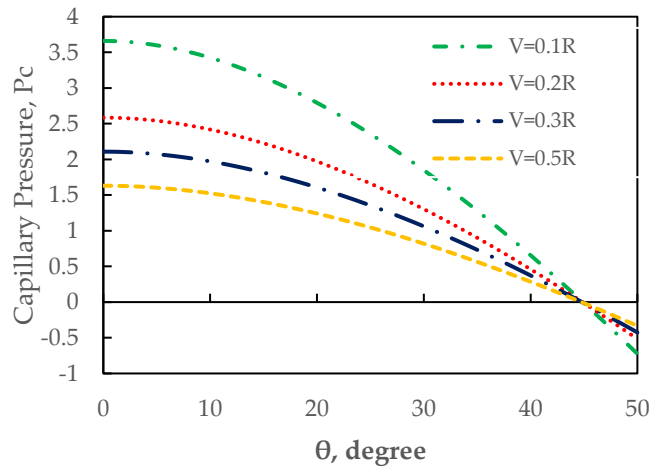
Finally, Figure 9(d) quantifies the error in the prediction for $R=50$ and different contact angles. The error is always small but increases weakly with contact angle and increase slightly with liquid volume.



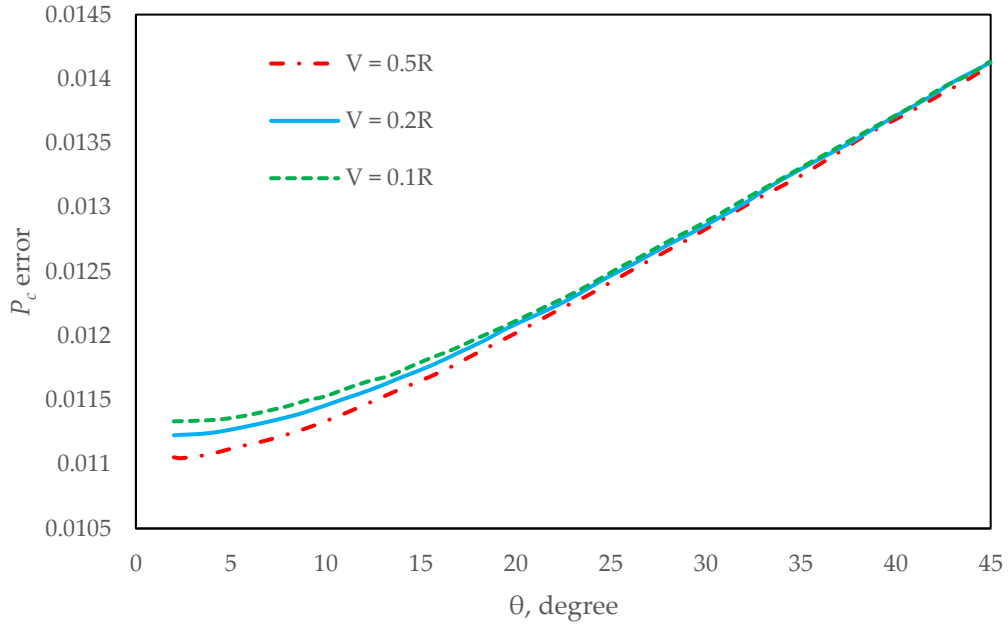
(a)



(b)



(c)



(d)

Figure 9. Effect of contact angle on the capillary pressure of the meniscus for (a) a fixed liquid volume ($V = 0.1R$) the capillary pressure for these two cylinder radii are compared with our prediction. Also shown are the interface shapes at three values of contact angle. (b) $R=1$ and (c) $R=50$ for different liquid volumes. (c) For (d) The capillary pressure error (Eq.(13)) for the case $R=50$ at different contact angles for various fixed liquid volumes.

4. Discussion and Conclusions

We have described numerical simulations and a predictive model for the shape of the meniscus surrounding the base of a circular cylinder attached to a flat horizontal substrate. In many ways, this is simpler than the more familiar problem of the capillary rise of liquid around a cylinder immersed in a liquid [11], and the different boundary condition at r_{\max} allows us to make progress

with a closed-form solution that works well at large R , i.e. cylinders that are many times wider than their height.

Notable features of the solutions we give are:

- The radial extent of the meniscus is much better described than the meniscus height by our solution; indeed, the width of the meniscus appears independent of cylinder radius;
- the critical contact angle at which the interface curvature/capillary pressure changes sign decreases with increasing cylinder radius;
- there is a particular contact angle at which the capillary pressure is the same irrespective of the meniscus volume;

The flow of liquids such as oil or water in porous media is a complex phenomenon determined by the characteristics of the reservoir. Moreover, as it is difficult to visualize fluid flow in subsurface formations, idealizing the pore channels to represent the real rock pores is necessary to understand the processes from a geological perspective. Our predictions should provide insight into reservoir simulation research as they provide a means to associate the characteristics of the rock structure with the capillary pressure and interface shapes.

Acknowledgments

SC thanks M.I.C. Teixeira and P.I.C. Teixeira for useful suggestions and K. Brakke for the development of the Surface Evolver. An AberDOC PhD scholarship from Aberystwyth University is gratefully acknowledged.

References

1. Cantat, I., Cohen-Addad, S., Elias, F., Graner, F., Höhler, R., Pitois, O., Rouyer, F. and Saint-Jalmes, A., **2013**. Foams: structure and dynamics. *OUP Oxford*.
2. Hassanizadeh, S.M. and Gray, W.G., **1993**. Thermodynamic basis of capillary pressure in porous media. *Water resources research*, 29(10), pp.3389-3405.
3. Soligno, G., Dijkstra, M. and van Roij, R., **2014**. The equilibrium shape of fluid-fluid interfaces: Derivation and a new numerical method for Young's and Young-Laplace equations. *The Journal of chemical physics*, 141(24), p.244702.
4. Wong, T.S., Sun, T., Feng, L. and Aizenberg, J., **2013**. Interfacial materials with special wettability. *MRS Bulletin*, 38(5), pp.366-371.
5. Rowlinson, J.S. and Widom, B., **2013**. Molecular theory of capillarity. *Courier Corporation*.
6. Xu, W., Ok, J.T., Xiao, F., Neeves, K.B. and Yin, X., **2014**. Effect of pore geometry and interfacial tension on water-oil displacement efficiency in oil-wet microfluidic porous media analogs. *Physics of fluids*, 26(9), p.093102.
7. Yeung, A., Dabros, T. and Masliyah, J., **1997**. Dissipative Interfaces and Departures from the Young-Laplace Equation. *Langmuir*, 13(24), pp.6597-6606.
8. Brakke, K.A., **1992**. The Surface Evolver. *Experimental mathematics*, 1(2), pp.141-165.
9. Hilden, J.L. and Trumble, K.P., **2003**. Numerical analysis of capillarity in packed spheres: Planar hexagonal-packed spheres. *Journal of colloid and interface science*, 267(2), pp.463-474.
10. Teixeira, M.A., Arscott, S., Cox, S.J. and Teixeira, P.I., **2015**. What is the shape of an air bubble on a liquid surface? *Langmuir*, 31(51), pp.13708-13717.
11. Howell, P.D., **1999**. The draining of a two-dimensional bubble. *Journal of Engineering Mathematics*, 35(3), pp.251-272.